Simulation of Semiconductor Processes and Devices 2016
Edited by E. Bär, J. Lorenz, and P. Pichler



# Automated Vertical Design Co-Optimization of a 1200V IGBT and Diode

M. Bina, A. Philippou, M. Hauf, Ch. Sandow, F.-J. Niedernostheide
Infineon Technologies AG
Am Campeon 1-12, D-85579 Neubiberg, Germany
Email: markus.bina@infineon.com

***Abstract*—In this work, we concentrate on extending our optimization method for IGBTs [1] in drives applications by incorporating diode parameters in addition to IGBT parameters. For this purpose, the fabrication process of the diode, including a platinum diffusion and it's parameters for lifetime adjustment [2], was added to the optimization loop. Consequently, the simulation of an IGBT turn-on event in the optimization loop was required.**

## I. Introduction

In our automated annealing algorithm described in [1], design optimization was done with a focus on the turn-off behavior of IGBTs for drives applications. Apart from the conduction losses, represented by the IGBT collector-emitter voltage, $V_{\mathrm{ce,sat}}$, at nominal conditions, the following key parameters of the turn-off transient were used for optimization: maximum collector-emitter voltage $V_{\mathrm{ce,max}}$, turn-off losses Eoff, and voltage rise rates $\frac{dV}{dt}$. The IGBT was optimized for lowest switching losses and modest overshoot voltages ($V_{\mathrm{ce,max}}$), combined with low $\frac{dV}{dt}|_{10,90}$, where the term $\frac{dV}{dt}|_{10,90}$ denotes a voltage gradient calculated from points taken at 10% and 90% DC Link voltage $V_{\mathrm{DC}}$ on the rising edge. These requirements on $\frac{dV}{dt}$ arise from electromagnetic compatibility (EMC) and interference (EMI) issues [3]. For most power applications, an optimized diode is also required for minimal losses and a favorable distribution of the turn-on losses between the IGBT ($E_{\mathrm{on}}$) and the diode ($E_{\mathrm{rec}}$). Thus, we extended our optimization algorithm by additionally taking into account key parameters characterizing the IGBT turn-on behavior and the diode turn-off behavior as well as the diode conduction losses. For IGBT optimization, we chose the same design parameters as described in detail in [1]: the field-stop profile consisting of the superposition of two gaussian profiles and the IGBT thickness. For the diode optimization, we chose the length and doping dose of a box-like field-stop profile at minimal device thickness, and to adjust the charge-carrier lifetime within the diode we used the platinum diffusion temperature within the model from [2]. However, other methods for charge-carrier lifetime adjustment, such as helium/hydrogen irradiation could be easily implemented in our algorithm as well. By carefully selecting the charge-carrier lifetime and the total field-stop charge, the on-state plasma distribution can be adjusted such that a balance between conduction losses and the switching behavior in terms of softness is achieved. However, an increased lifetime killing also increases the diode conduction losses. A similar trade-off can be found for the field-stop. A thicker or higher doped field-stop yields a higher total stored charge in the diode while it allows the use of a thinner intrinsic region in the device.

## II. Simulation Approach

In the modified simulated annealing iteration scheme of the optimizer, a simplified chopper circuit was used for both IGBT turn-on and turn-off simulations utilizing the device simulator *Sentaurus Device*. The chopper circuit, including circuit parameters common to all simulation runs, is shown in Fig. 1. The IGBT turn-off behavior was optimized for turn-off transients at a DC link voltage of $800\,\mathrm{V}$ ($V_{\mathrm{CC}}$) at $25\,^{\circ}\mathrm{C}$ and nominal current $I_{\mathrm{nom}}$. Additionally, the IGBT turn-on behavior together with the turn-off behavior of the diode was optimized for $V_{\mathrm{CC}} = 600\,\mathrm{V}$ at $175\,^{\circ}\mathrm{C}$ and $I_{\mathrm{nom}}$. For each iteration of the modified simulated annealing scheme, both simulation runs were performed at a low gate resistance $R_{\mathrm{g}}$ of $2\,\Omega$. After both simulations were completed several evaluation parameters were extracted from the simulation results. Apart from the conduction losses, represented by the IGBT collector-emitter voltage, $V_{\mathrm{ce,sat}}$ at nominal conditions, the following key parameters of the turn-off transient were used for optimization:

- turn-off losses $E_{\mathrm{off}}$,
- $\frac{dV}{dt}|_{10,90}$,
- collector-emitter ringing voltage $V_r$ and
- maximum collector-emitter voltage $V_{\mathrm{ce,max}}$.

The collector-emitter ringing voltage is defined as the amplitude of the first half cycle of the excited $V_{\mathrm{ce}}$ oscillation appearing after the voltage overshoot during turn off (for details cf. [1]). For the turn-on event of the IGBT and the diode turn-off characteristic the following parameters were used for optimization:

- IGBT turn-on losses $E_{\mathrm{on}}$,
- voltage rise rates $\frac{dV}{dt}$,
- diode maximum reverse current $I_{\mathrm{rrm}}$,
- diode recovery losses $E_{\mathrm{rec}}$ and
- diode reverse recovery charge $Q_{\mathrm{rr}}$.

For the voltage rise rates an error function was utilized in order to implement a more relaxed and soft $5\,\frac{kV}{\mu s}$ constraint, where the error to be minimized increased with voltage rise rates above the target of $5\,\frac{kV}{\mu s}$. For the IGBT softness evaluation

we used the same approach as described in [1], whereas the diode softness was evaluated using $I_{\mathrm{rrm}}$ and $Q_{\mathrm{rr}}$. An overview of the evaluation parameters and their constraints is given in Tab. I. The field-stop profile of the IGBT was

TABLE I
EVALUATION PARAMETERS

| | $\frac{dV}{dt}\|_{10,90}$ | $V_{\mathrm{ce,max}}$ | $V_{\mathrm{r}}$ | $V_{\mathrm{ce,sat}}$ | $E_{\mathrm{off}}$ |
|---|---|---|---|---|---|
| Unit | $\frac{kV}{\mu s}$ | $V$ | $V$ | $V$ | $mJ$ |
| Constraint | $< 5.0$ (soft) | $< 1150$ | $< 20$ | 1.4 | 5 |
| | $E_{\mathrm{rec}}$ | $Q_{\mathrm{rr}}$ | $I_{\mathrm{rrm}}$ | $V_{\mathrm{F}}$ | $E_{\mathrm{on}}$ |
| Unit | $mJ$ | $As$ | $A$ | $V$ | $mJ$ |
| Constraint | $< 5$ | $< 15$ | $< 350$ | 1.7 | 5 |

parametrized via the superposition of two Gaussian functions $G_1(\sigma_1, x_1 = 0, N_1)$ and $G_2(\sigma_2, x_2, N_2)$, where $\sigma$ denotes the standard deviation, $x$ the central position of the Gaussian function in $\mu m$ from the backside, and $N$ the peak concentration of the respective Gaussian function (Fig. 2 bottom). The position of $G_1$ was fixed to the backside, as a final peak in front of the collector-side p-doping layer is necessary for a field-stop IGBT to prevent a punch-through. Further optimization parameters included the collector-side p-doping dose $d_{\mathrm{p}}$ and the device thickness $x_{\mathrm{w}}$ which was adjusted to fulfill the breakdown voltage requirements of a 1200 V IGBT. For the diode, the width $w$ and height $f_{\mathrm{d}}$ of a box-shaped field-stop profile was used as optimization parameters (Fig. 2 top). The thickness of the device was fixed and the integral field-stop dose was limited such that the breakdown voltage requirements of a 1200 V diode could not be violated during optimization. Additionally, we utilized the approach from [2] to simulate the resulting charge-carrier lifetime resulting from platinum diffusion. The diffusion temperature $T_{P,\,diff}$ was used as an optimization parameter. A possible resulting profile of deep trap levels using this approach is shown in Fig. 2 top. The higher the deep level concentration, the smaller is the charge-carrier lifetime. The trapping model of choice is the Shockley-Read-Hall model [4]. The optimization parameters are shown in Tab. II. Three different runs were carried out to test our

TABLE II
OPTIMIZATION PARAMETERS

| | $N_2$ | $N_1$ | $\sigma_2$ | $x_2$ | $\sigma_1$ |
|---|---|---|---|---|---|
| Unit | $cm^{-3}$ | $cm^{-3}$ | $\mu m$ | $\mu m$ | $\mu m$ |
| Min: | $N_{min}$ | $N_{min}$ | 1 | 1 | 1 |
| Max: | $30 \times N_{min}$ | $60 \times N_{min}$ | 20 | 39 | 20 |
| | $d_p$ | $f_{\mathrm{p}}$ | $w$ | $T_{P,\,diff}$ | |
| Unit | $cm^{-2}$ | $cm^{-3}$ | $\mu m$ | $K$ | |
| Min: | $0.2 \times 10^{13}$ | $N_{min}$ | 10 | $T_{P\,0}$ | |
| Max: | $2.4 \times 10^{13}$ | $200 \times N_{min}$ | 40 | $T_{P\,0} + 100\mathrm{K}$ | |

optimization concept. In Run A, only the diode was optimized. The IGBT for this run remained unchanged and was the same as the high-power variant in [1], but with a stray inductance of

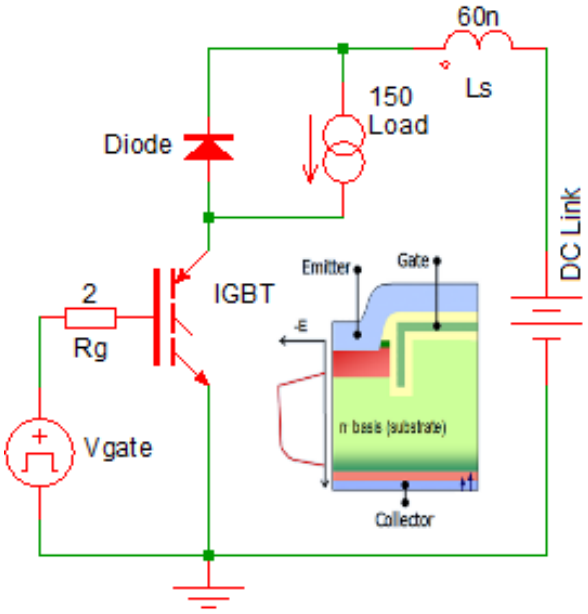


Fig. 1. Chopper circuit together with a schematic of the IGBT cell used for simulations during each optimization iteration.

60 nH. In Run B, the IGBT was co-optimized with the diode, however the diode parameters $Q_{\mathrm{rr}}$ and $I_{\mathrm{rrm}}$ were not taken into account. In Run C, both diode and IGBT were optimized including a minimization of $Q_{\mathrm{rr}}$ and $I_{\mathrm{rrm}}$. All optimization runs were performed with 250 iterations each, where each iteration took around 12 minutes.

## III. RESULTS

Fig. 3 shows the target function value and the annealing temperature for all three runs. In Run A, the target function could not be reduced further. However, when the IGBT was co-optimized together with the diode including the diode parameters $V_{\mathrm{F}}$ and $E_{\mathrm{rec}}$ (Run B), a lower target function value than in Run A can be found. When all evaluation parameters were taken into account including $Q_{\mathrm{rr}}$ and $I_{\mathrm{rrm}}$ (Run C), a similar target function value as in Run B was achieved. The turn-on transients and key figures are shown in Fig. 4 and Fig. 5. For turn-off, the transients and key figures are shown in Fig. 6 and Fig. 7, respectively. Since the IGBT turn-on current transient is essentially determined by the diode turn-off behavior as soon as the current level has reached the target level (in Fig. 4 $I_{\mathrm{nom}}$), the diode turn-off behavior can be assessed by inspecting the IGBT turn-on transient. Run A yielded a soft switching IGBT and diode, resulting in the lowest $V_{\mathrm{ce,sat}}$ and $I_{\mathrm{rrm}}$ of all runs. However, the switching losses are higher because of the large current tails, which are visible in the turn-off and turn-on transients. Run B shows that by co-optimizing diode and IGBT still a soft switching behavior at the cost of a higher $V_{\mathrm{ce,max}}$ and $I_{\mathrm{rrm}}$ could be achieved. Run C is the most aggressively optimized variant, which can be readily seen in the large $V_{\mathrm{ce,max}}$. The increasing $V_{\mathrm{ce,max}}$ from Run A to Run C reflects the different thicknesses of the IGBTs, which is

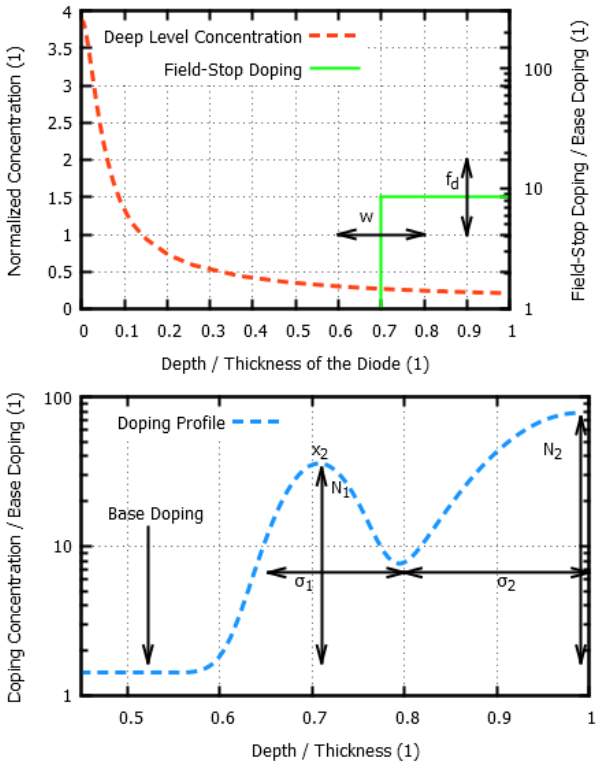


Fig. 2. **Top**: The exemplary concentration of deep levels due to the platinum diffusion. Depending on the platinum temperature $T_{P,diff}$ the anode side charge-carrier concentration can be changed in a fully flooded diode. Additionally, the box-shaped field-stop and its parameters used in the simulation is shown. **Bottom**: Examplary field-stop profile consisting of the superposition of two Gaussian distributions with the corresponding parameters.

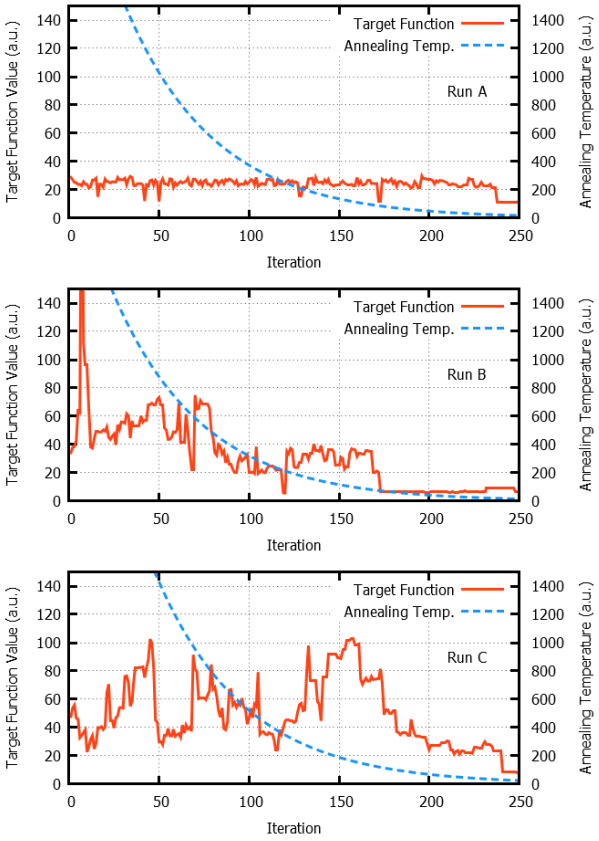


Fig. 3. Iterations in a simulated annealing optimization scheme. **Top**: For Run A, only the diode was optimized using the high-power IGBT from [1]. As can be seen the target function value of this variant was already close to the optimum. **Middle**: In Run B, IGBT and diode were co-optimized, disregarding $Q_{\mathrm{rr}}$. An optimum was found after 110 iterations. **Bottom**: In Run C, all parameters were evaluated in a co-optimization. An optimum was found with a target function value close to that of Run B.

10% and 13% lower in the optimized variants of Run B and C compared with Run A. The diodes resulting from Run A, B, C have a $V_{\mathrm{F}}$ of 1.7 V, 1.5 V and 1.6 V, respectively at 175 °C. Comparing the turn-on transients, one can clearly see that the most aggressive optimization (Run C) yields the best results of all three runs. Depending on the application, either the IGBT/diode combination from Run B, for applications requiring a softer switching behavior, or from Run C, for fast switching applications, is the best choice. Altogether, our results show that a simultaneous co-optimization of IGBT and diode with our optimization algorithm yields significant better results than a serial and separate optimization of the IGBT and the diode.

## IV. Conclusion

In this work we showed that a co-optimization can yield optimal IGBT and diode combinations, depending on the optimization scheme chosen according to the application-specific requirements. For example, by setting a target for the diode recovery charge one can choose between a soft (Run B) or more aggressive version (Run C) of the same technology. With a minimal increase of the simulation time from 10 to 12 minutes per iteration by including the diode optimization we can successfully tackle the complex, nonlinear and high dimensional co-optimization of IGBT and diode. While we minimized the number of evaluation parameters, to the most important switching parameters of the IGBT and the diode, other parameters such as cosmic ray FIT-rates [5] and short-circuit requirements can be easily incorporated into the algorithm.

## References

[1] A. Philippou, M. Bina, F.-J. Niedernostheide, *Automated Vertical Design Optimization of a 1200V IGBT*, Proc. SISPAD'15, 2015.
[2] E. Badr, P. Pichler, G. Schmidt, *Extended model for platinum diffusion in silicon*, PRIME, 2013.
[3] Q. Lid, W. Shen, F. Wang, D. Boroyevich, V. Stefanovic, M. Arpilliere, *Experimental Evaluation of IGBTs for Characterizing and Modeling Conducted EMI Emission in PWM Inverters*, Power Electronics Specialists Conference, vol. 4., pp. 1951-1956, 2003.
[4] W. Shockley, W. Read, *Statistics of the Recombinations of Holes and Electrons*, PR, vol. 87, no. 5, pp. 835842, 1952.
[5] F. Pfirsch, G. Soelkner, *Simulation of cosmic ray failures rates using semiempirical models*, ISPSD, 2010, pp. 125-128.

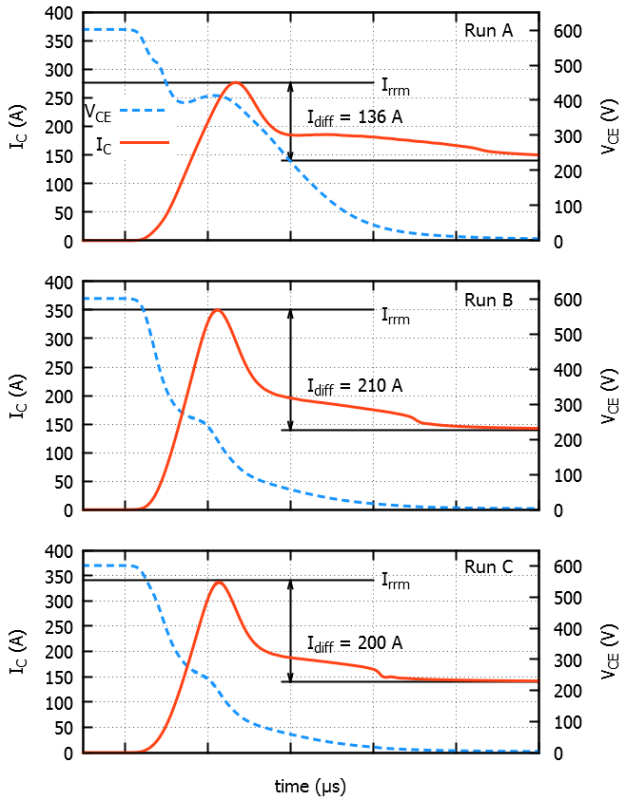


Fig. 4. Turn-on switching characteristic of the optimized IGBTs and respective diodes from Run A (top) to Run C (bottom). While the IGBT and diode resulting from Run A show a large current tail and thus very soft switching behavior, the IGTBs and diodes from Run B and Run C show a smaller current tail and higher $I_{\mathrm{rrm}}$, at the cost of slight increase in $V_{\mathrm{diff}}$ (Fig. 5).

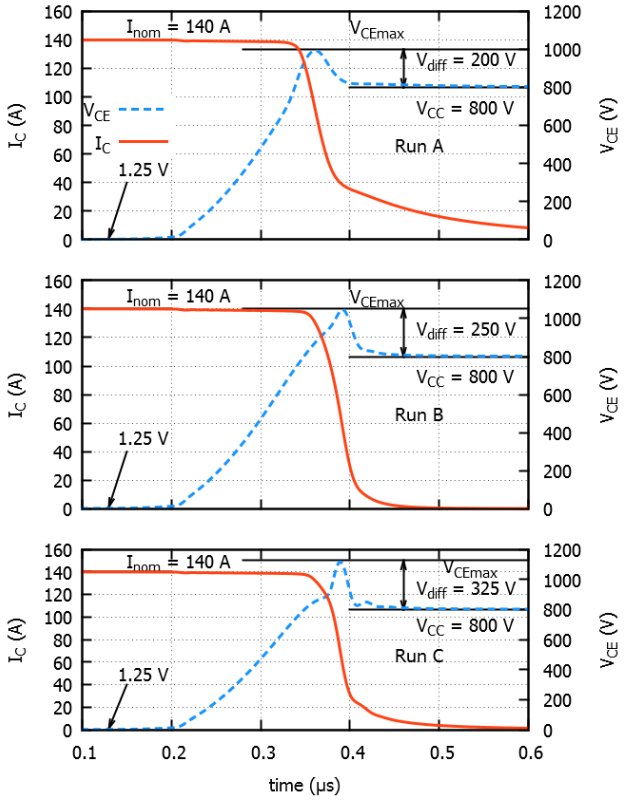


Fig. 6. Turn-off switching characteristic of the optimized IGBTs and diodes from Run A (top) to Run C (bottom). Run C resulted in an aggressively scaled IGBT and diode with higher $V_{\mathrm{diff}}$ than all other variants. Additionally, IGBT and diode of Run C show a characteristic voltage peak and a unsoft turn-off behavior, compared to the devices from Run A and B.

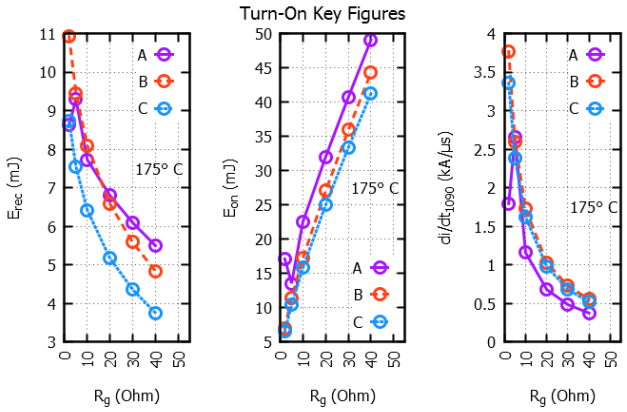


Fig. 5. Key figures for turn-on over $R_{\mathrm{g}}$ of the optimized devices at 175 °C. The devices from all runs show the same qualitative behavior for $E_{\mathrm{on}}$, $\frac{dI}{dt}$ and $\frac{dV}{dt}$. For turn-on the IGBT and diode combination from Run C yields the better results.

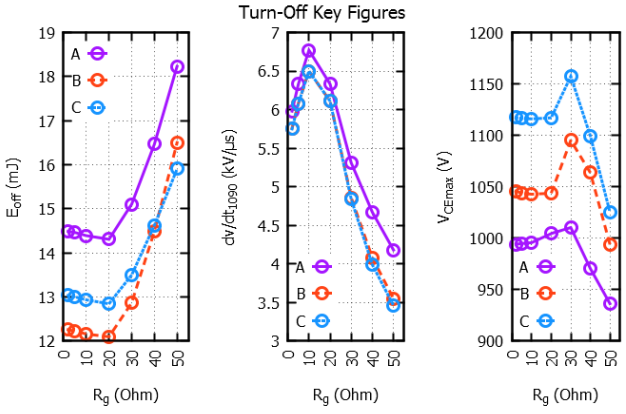


Fig. 7. Key figures for turn-off over $R_{\mathrm{g}}$ of the optimized devices for turn-off at 25 °C. The devices from all runs show the same qualitative behavior for $E_{\mathrm{off}}$, $\frac{dI}{dt}$ and $\frac{dV}{dt}$. With a higher $R_{\mathrm{g}}$, $E_{\mathrm{off}}$ rises while $\frac{dV}{dt}|_{10,90}$ and $\frac{dI}{dt}|_{10,90}$ fall. Additionally, the IGBT and diode combination of Run B performs best in turn-off with the lowest $V_{\mathrm{F}}$ at 175 °C of 1.5 V. However, for turn-on the IGBT and diode combination from Run C yields the better results (Fig. 5).